Crazelike Features in Deformation of Hard Elastic Poly(4-Methyl-1-Pentene) Film

TETSUYA TANIGAMI,* KAZUO YAMAURA, and SHUJI MATSUZAWA, *Department of Chemistry, Faculty of Textile Science and Technology, Shinshu University, Ueda, Nagano-ken 386, Japan,* and KENJI OHSAWA and KEIZO MIYASAKA, *Department of Textile and Polymeric Materials, Tokyo Institute of Technology, Ookayama, Meguro-ku, Tokyo 152, Japan*

Synopsis

A hard elastic film of poly(4-methyl-1-pentene) was investigated by using wide-angle X-ray diffraction, small-angle X-ray scattering (SAXS), and stress–strain measurements. The film showed somewhat hard elasticity above the glass transition temperature (T_g), while it showed a brittle nature below T_g. In the former case, the SAXS pattern of the stretched film was very analogous to that of usual crazed materials (crazelike feature), namely void scattering on the meridian and interference scattering due to microfibrils on the equator. The fibrillation was discussed in terms of deformability of the lamellae and, further, that of the helical chain. Our results were also compared with the model of Čačković and Hosemann for deformation of hard elastic crystalline materials.

INTRODUCTION

"Hard" elastic materials have been investigated for many polymers.[1–3] Hard elastic polypropylene (HEPP) have been most warmly attracting many investigators, not only for its excellent industrial use but also for its scientifically interesting properties. However, it should be noted that the hard elasticity has been given to many other polymers, although the degree of hard elasticity of them, which has been usually defined as large strain recoverability on uniaxially stretching, was not so conspicuous as that of HEPP. The common structural feature of the hard elastic materials is one-dimensional stacks of laterally well-developed lamellae, in the case that their constituent polymers are crystallizable.

On the other hand, the deformation mechanisms of amorphous and poorly crystallizable polymers have been energetically studied in terms of crazing,[4] and it was rarely the case that the crazing was related to the strain recoverability, probably because of their low recoverability with some exceptions such as high-impact polystyrene[5] and polycarbonate.[6] Void formation appeared on stretching specimens is a common feature between the crystalline hard elastic and the crazed materials. Thus, we expected that some crystalline hard elastic materials would be useful to investigate the crazing mechanism, because the structure of the former could be regarded as simplified ones for the crazed materials. The structural simplicity is based on

* To whom correspondence should be addressed.

Journal of Applied Polymer Science, Vol. 32, 4491–4502 (1986)
 CCC 0021-8995/86/044491-12$04.00

highly oriented molecules and clearly separated two phases, namely, alternating structure of the lamellae and the amorphous layers. For our purpose, HEPP is not preferable, because its strain recoverability is so high that it seems not to be analogous to the crazed materials. Recently, we found the good structural similarity in a hard elastic film of poly(4-methyl-1-pentene) (P4M1P), and briefly report on this in this paper. Although Noether and Whitney[7] had reported on HEP4M1P, we investigate more precisely in this work.

The hard elasticity of the "HE"-P4M1P was very poor. To ascertain the reason for this poor elasticity is another aim in this paper. P4M1P has been considered to be a peculiar polymer, for the lower density of the crystal phase than the amorphous one at room temperature.[8,9] Further, the low crystal density is due to the loosely spiraled chain with the bulky side chain of isobutyl group. As expected from these structural aspects, the elastic modulus is so small in the chain direction, as well as in the lateral direction with respect to the chain axis, that the lamella itself would be also easily deformed.[10] We will discuss the hard elasticity in terms of lamellar deformation.

EXPERIMENTAL

Sample Preparation

P4M1P pellets (TPX, Mitsui Petrochemical Co. Ltd., Japan) were used for this study. A thin film 6 μm thick and 20 cm wide was prepared from the molten pellets, by the use of an extruder with a T-die. The temperature of the melt was 250°C, and the extruded melt was cooled to be taken up at a speed of 1 m s^{-1}. In order to develop the crystallinity, the film was annealed at 210°C for 1 h. The annealing at this temperature has been ascertained to be effective on the increase of crystallinity.[9]

Measurements

Stress–strain curves were recorded using a "Tensilon" tensile-tester (model UTM-III, Toyo Baldwin Co., Japan) equipped with a temperature-controlled oven. The initial length of the specimens was 30 mm and the width was 3 mm. Extension rate was 4 mm min^{-1}.

Wide-angle X-ray diffraction (WAXD) photograph and intensity curves were obtained by using a Rigaku Denki D3 type apparatus.

Small angle X-ray scattering (SAXS) photographs and intensity curves were obtained by using a Rigaku-Denki RU-3 type apparatus. The SAXS intensity curves were measured along the meridional and the equatorial directions, i.e., directions parallel and normal to extrusion direction (ED), respectively, with line focussing under the following collimating system: The second slit, the specimen, and the third and fourth slits which were placed, respectively, in front of and behind the soller slits were placed at 228.5, 272, 592, and 659 mm for the first slit, respectively, and the sizes of the first, second, third, and fourth slits were 0.2 × 11, 0.1 × 11, 0.1 × 11 and 0.05 × 15 mm^2, respectively. The SAXS photographs were taken with

a point focussing system under the following collimations: Distances of the second pinhole, specimen, and a photographic film were 228.5, 272, and 659 mm from the first pinhole, respectively, and the sizes of the first and second pinholes were 0.2 and 0.1 mm, respectively.

Temperature control of the specimen to obtain the SAXS intensity curve at 150°C in Figure 5 was performed by blowing heated nitrogen gas over the specimen. Stretching of the specimen for the X-ray measurements was performed in the sample holder at 30°C, which was the same as the measuring temperature.

ESTIMATION OF CRYSTALLINITY AND MOLECULAR ORIENTATION

Crystallinity

The crystallinity of the sample was estimated from WAXD intensity curve as described previously.[9] On measuring this curve, the oriented specimen was rotated in the plane normal to X-ray beam by using a rotating equipment, in order to put out the molecular orientation effect on the estimation.

Molecular Orientation

The degree of crystalline molecular orientation was estimated from the profile of the 200 reflection. From the profile which was measured in the azimuthal angle, the mean value of $\cos^2 \theta_{200}$ was calculated, where θ_{200} was the angle between ED and the normal of the (200) plane. The orientation factor of the *c*-axis (chain axis) with respect to ED was calculated by the following equations[11]:

$$f_c = (3 \cos^2 \theta_c - 1)/2 \tag{1}$$

$$\cos^2 \theta_c = 1 - 2 \cos^2 \theta_{200} \tag{2}$$

where θ_c is the angle between ED and the *c*-axis.

RESULTS

Mechanical Properties

The glass transition point (T_g) of P4M1P is near room temperature.[8] The transition much effected on the mechanical property as shown in Figure 1. Above T_g the specimen showed the large length recovery from 50% extension. On the other hand, below T_g, it showed brittle nature. This indicates that, at T_g, the elastic modulus of the amorphous phase decreases smaller than a critical value below which the hard elasticity appears. The observed values of the recovery % from 50% extension above T_g, ER_{50} = 50–70%, were smaller than the reported values ER_{100} > 95% for the hard elastic materials[7,12–14] such as PP and polyoxymethylene. Thus, strictly speaking, the P4M1P film prepared by us cannot be regarded as a good hard elastic one.

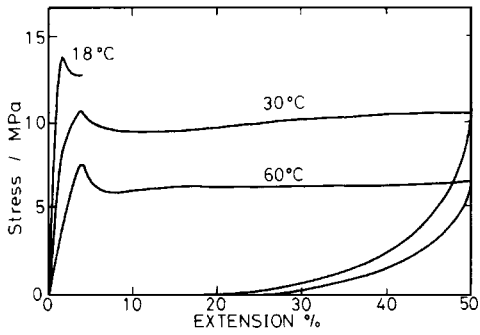

Fig. 1. Stress–strain behavior of the P4M1P sample at various temperatures. The tensile direction was parallel to ED.

WIDE-ANGLE X-RAY DIFFRACTION

Figure 2 shows the WAXD pattern of the unstretched film. The degree of the crystal orientation and sharpness of the diffraction arcs were almost the same as those observed in the usual hard elastic films. The half width and the spacing were obtained from the 200 diffraction profile in 2θ angle as a function of extension, as shown in Figure 3. The d_{200} vs. extension curve showed similar behavior to the stress vs. extension curve in Figure 1. The d_{200} firstly decreased with extension to the minimum point at about 3% extension, which corresponded to the yielding point observed in the stress-extension curve in Figure 1. This lateral shrinkage of the lattice can be related to that of the helical chain itself, as mentioned in Discussion section. The half width monotonously but slightly increased with increasing extension. This is due to subdivision of the lamella associating with decrease of the lamellar lateral size, as also mentioned later. The orientation factor slightly decreased with increasing extension above the yielding point as shown in Figure 4, but the decrease was considered to be almost negligible.

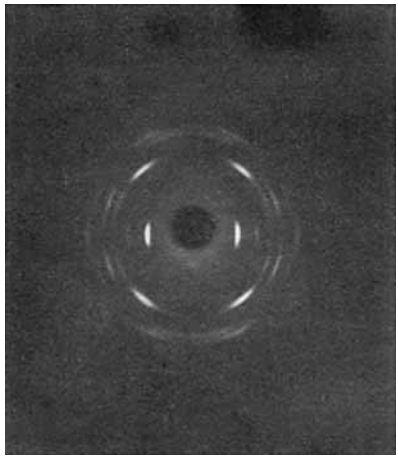

Fig. 2. WAXD photograph of the unstretched sample. The extrusion direction is vertical.

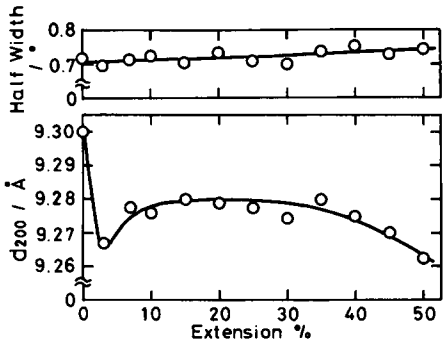

Fig. 3. Spacing of the (200)-plane and half width of the 200 reflection profile, which was measured in 2θ angle, are shown as a function of extension.

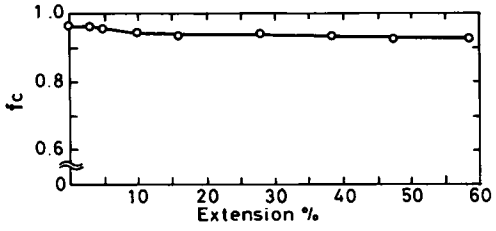

Fig. 4. The change of the orientation factor f_c of the crystal c-axis with extension.

SMALL-ANGLE X-RAY SCATTERING

As reported previously,[8,9] the density difference between the crystal phase and the amorphous one is so small in P4M1P that the interlamellar scattering cannot be detected at room temperature by using a general apparatus. Thus we used the heating method[9] to detect it. Figure 5 shows the SAXS intensity curves measured at 20 and 150°C. The interlamellar spacing was calculated from the latter curve to be 330 Å. The crystallinity was measured

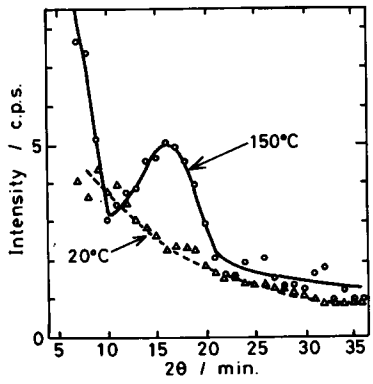

Fig. 5. Meridional SAXS intensity curves of the unstretched sample measured at 20 and 150°C.

to be 50%. The size of the lamellae in ED was roughly estimated to be 165 Å by using the spacing and the crystallinity.

Figure 6 shows the change of the SAXS pattern with extension at 30°C. Two types of scatterings appeared with increasing extension. One was the intense meridional one which was usually due to microvoid formation on stretching of the hard elastic materials. Another was the anomalous equatorial scattering which was very streaky and had a maximum. The two scattering was remained in the relaxed sample as Figure 6(e) shows. This indicates that the void formation and the fibrillation partly have the nature of plastic deformation. We will individually discuss the two scatterings. It should be noticed that the interference scattering between the crystal and amorphous phases cannot appear in P4M1P, even if the annealed sample is stretched.

Meridional Scattering

Figure 7 shows the meridional SAXS intensity curves at various extensions. Two orders of magnitude of increase in the intensity with increasing extension up to 8% indicates that the greater part of the microvoids were formed in the early stage of stretching. It should be noticed that the intensity curve of the unstretched sample in this case was almost the same as that in Figure 5 and not drawn in Figure 7. The monotonous decrease of the intensity with increasing 2θ angle observed at all extensions indicates much irregular void formation. In the usual hard elastic materials, however, the meridional scattering shows two-spot pattern due to the intervoid interference scattering. The void formation was also observed as whitening of the specimen.

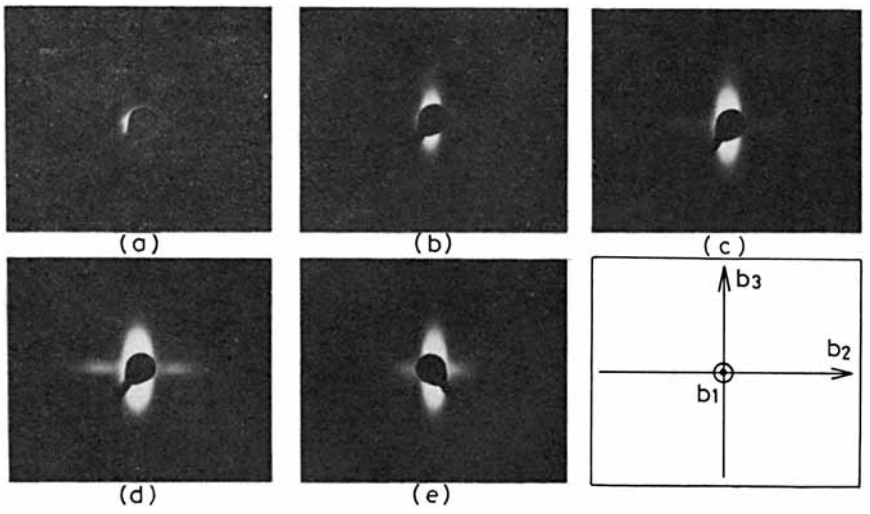

Fig. 6. SAXS photographs taken at 30°C from the stretched and the unstretched samples. Extension is (a) 0%, (b) 8%, (c) 23%, and (d) 40%. (e) is for the relaxed sample after stretching to 40% extension.

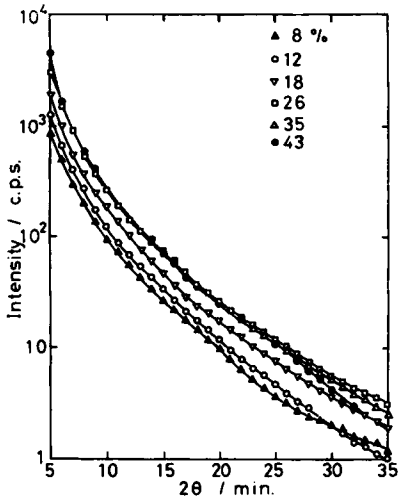

Fig. 7. Change of the meridional SAXS intensity curve with extension at 30°C. The numbers on the curves indicate extension (%): (▲) 8; (○) 12; (▽) 18; (□) 26; (△) 35; (●) 43.

Equatorial Scattering

Figure 8 shows a change of the equatorial SAXS intensity curve with increasing extension. The intensity gradually increased with extension, but it was two or three orders of magnitude smaller than the meridional intensity. The peak was due to the formation of the fibril parallel to ED. Although the equatorial interfibrillar scattering has been observed in some hard elastic materials such as PP,[7] it seems to be rarely the case that the interfibrillar interference maximum appeared. On the other hand, a couple of the void scattering and the interfibrillar scattering has been often observed in crazing of PS,[15,17] poly(methyl methacrylate),[16] and poly(vinyl alcohol),[17] etc.

Figure 9 shows a change of the interfibrillar spacing calculated from Figure 8 with extension. In our measurements, it took long time to scan the

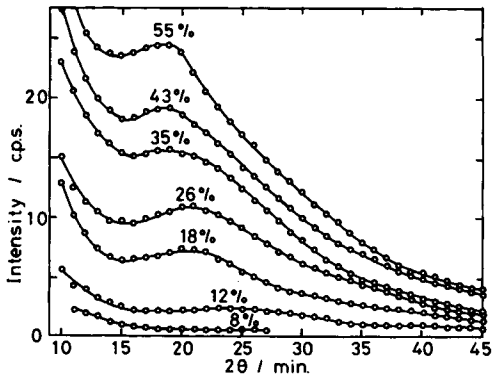

Fig. 8. Change of the equatorial SAXS intensity curve with extension at 30°C. The numbers on the curves indicate extension %.

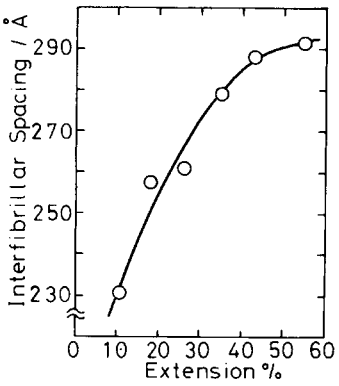

Fig. 9. Change of the interfibrillar spacing calculated from the peak positions of the equatorial SAXS curves in Figure 8 with extension.

SAXS intensity so that the actual change would be different from our results, especially in the initial stage of stretching. The large spacing at high extensions may be caused by decreasing of the number of fibrils due to break, and/or by bundling of small fibrils.

DISCUSSION

Monotonously decreasing SAXS intensity curves as the meridional intensity curves in Figure 7 have been analyzed by the generalized Guinier approximation.[18] Consider rectangular Cartesian coordinate axes $X_1X_2X_3$ (Fig. 10). The reciprocal coordinate axes $b_1b_2b_3$ is also represented in the figure. The one-dimensional alternating stack of the lamellae and the amorphous layers are aligned in direction of the X_3-axis. We assume that the microvoids which have the uniform surface area $(L_1 \times L_2)$ are randomly formed in some of the interlamellar regions as shown in Figure 10. The

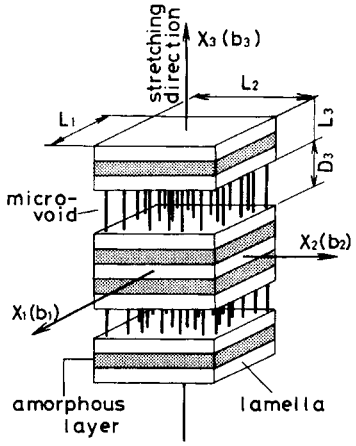

Fig. 10. Schematic drawing of the elements of a crazelike scattering model.

lateral sizes of the voids (L_1 and L_2) were considered to be larger than the size in ED, since the size in direction of the b_2-axis of the meridional void scattering was very narrow, as shown in Figure 6. The meridional scattering of the microvoids is expressed by the following equation:

$$I(0, 0, b_3) \sim N (\Delta\rho)^2 v^2 \exp\left[-\frac{1}{3}\pi^2 D_3^2 b_3^2 \right] \tag{3}$$

where N is the number of the void, $\Delta\rho$ is the density difference between the void and the polymer, v is volume of the void, and D_3 is the mean length of the voids in direction of the X_3-axis. If the voids are divided into some groups depending on the size, eq. (3) is rewritten as follows:

$$I(b_3) \sim (\Delta\rho)^2 \sum_j N_j v_j^2 \exp\left[-\frac{1}{3}\pi^2 D_{3,j}^2 b_3^2 \right] \tag{4}$$

Figure 11 shows the Guinier plot, namely, log $I(0, 0, b_3)$ vs. b_3^2 plot, for the specimen with 35% extension. Here, eq. (4) is used to obtain the mean void length D_3. The voids contained in the specimen are divided into four groups depending on the values of D_3, which are presented by the four lines in Figure 11. Figure 12 shows the D_3 value which is calculated from the line in the lowest b_3 range. It shows that the void formation was performed below about 10% extension, and that the void size in direction of the X_3-axis is larger than that observed in HEPP.[13,14] The latter fact indicates the localized void formation in HEP4M1P. The numerical fractions of the voids with the same D_3 value can be calculated from the values at the intersections of the Guinier plot lines, such as the lines 1–4 in Figure 11, with the vertical axis. Figure 13 shows the distribution function of D_3 calculated by eq. (4) for the various extensions. Significant change is not observed in the distributions.

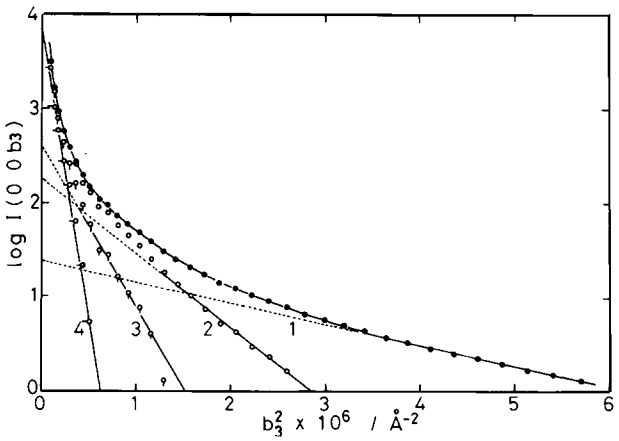

Fig. 11. The Guinier plot of the meridional SAXS intensity curve at 35% extension.

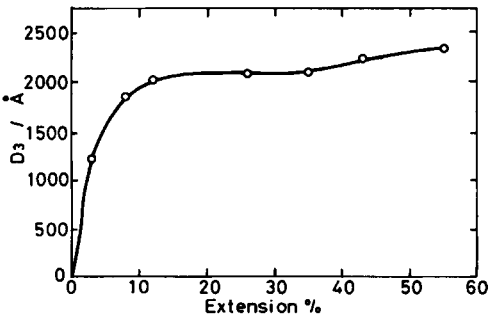

Fig. 12. Change of D_3 with extension.

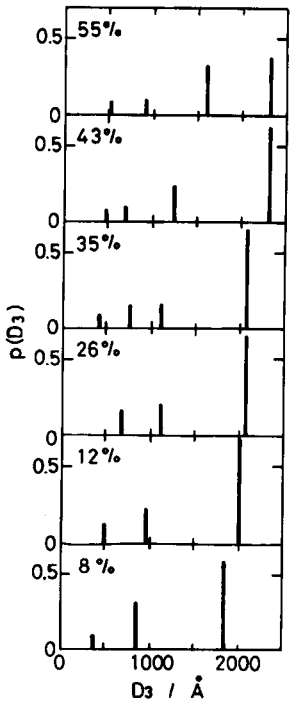

Fig. 13. Distributions of D_3 for various extensions.

The equatorial interference scattering must be caused by the fibrillation. The interlamellar fibril may be composed of not only the amorphous molecules but also the destructed lamellae. It seems that the lamellae are easily deformed by the shear stress along the chain axis, and destructed into many pieces of smaller lamellae. The unchanged crystal orientation on the stretching (in Fig. 4) supports the destructions by the shear stress. The broadening of the half width of the 200 reflection with stretching (in Fig. 3) indicates the decrease of the lateral size of the lamellae. The lamellae which were not destructed into fibrils must be also deformed into somewhat smaller lamellae, although the lamellae are illustrated as if they are not deformed in Figure 10.

Čačković et al. studied on hard elastic materials based on nuclear magnetic resonance measurements and proposed a new deformation model for the stacked lamellae.[19,20] Their model is very analogous to our idea especially on the three points: First, there are destructible and indestructible microparacrystals (dmPCs and imPCs). Secondly, the lamella are deformed by shear stress on stretching. Lastly, further stretching introduces fibrillation from dmPCs. Their model was very precisely expressed by an illustration (Fig. 1 in Ref. 19). They further mentioned that the excess energy of the large free surface of the fibrils produces the reverse driving force (hard elasticity). This explanation of the driving force is different from the most of other investigators ideas,[2] in which bending of lamellae is several times considered to be main contribution to hard elasticity. However, it should be noticed that, in our HEP4M1P film, fibrillation did not successfully act as the driving force. The fraction of the dmPCs in our film would be so small that the fibrillation locally proceeded to plastic deformation or breaking regions. This seems to be one reason for the poor hard elasticity.

The 7/2 helical chain is easily strained not only along the chain axis but also in lateral direction of the chain on stretching along the chain axis. The deformations in the two directions are relevant to each other: extension along the chain axis and shrinkage in the lateral direction, and vice versa. The relevancy was also reported on the thermal expansibility of the chain.[21] Thus, the lamellae in HEP4M1P film would be more easily subdivided than in other HE films, owing to the large lateral shrinkage of the individual 7/2 helical chains on stretching. Small pieces of the subdivided lamellae would be further converted into fine fibrils, keeping a somewhat lamellar nature. The high deformability of the chain may cause plastic deformation and breakdown of the fibrils. The fibrillation mechanism from the lamellae was more precisely discussed by Kausch.[22]

CONCLUSIONS

1. A P4M1P film prepared by melt extrusion under tension showed hard elasticity above the glass transition point (T_g), while it behaved as a brittle film below T_g. This means that the modulus of the amorphous phase must be lower than a critical value to show the hard elasticity.

2. The hard elastic deformation of P4M1P was shown to be very similar to that in crazed materials with regard to small-angle X-ray scattering (see Fig. 6). The SAXS pattern for the stretched HEP4M1P was composed of two parts: one was normal void scattering on the meridian; another was anomalous streaky scattering on the equator. The latter is interfibrillar interference scattering, and the fibril was formed in the microvoids.

3. The high interference scattering between the fibrils detected on equatorial SAXS profiles (see Fig. 8) indicated that the greater part of fibrillation may be due to subdivision of the lamellae caused by shear stress along the ED. Further, it could be related to easiness of shrinkage of the helical chain in the lateral direction on stretching along the chain axis. The fibrillation with plastic deformation or break down must be one reason for the poor hard elasticity.

References

1. H. D. Noether, *Flow-Induced Crystallization in Polymer Systems*, R. L. Miller, Ed., Gordon and Breach, New York, 1979, p. 217.
2. S. L. Cannon, G. B. MaKenna, and W. O. Statton, *J. Polym. Sci. Macromol. Rev.*, **11**, 209 (1976).
3. B. S. Sprague, *J. Macromol. Sci. Phys.*, **B8**, 157 (1973).
4. *Crazing in Polymers*, Advances in Polymer Science 52/53, H. H. Kausch, Ed., Springer-Verlag, Berlin, 1983.
5. A. Moet, I. Palley, and E. Baer. *J. Appl. Phys.*, **51**, 5175 (1980).
6. R. P. Kambour and R. W. Kopp, *J. Polym. Sci., A-2*, **7**, 183 (1969).
7. H. D. Noether and W. Whitney, *Kolloid Z. Z. Polym.*, **251**, 991 (1973).
8. J. H. Griffith and B. G. Rånby, *J. Polym. Sci.*, **44**, 369 (1966).
9. T. Tanigami and K. Miyasaka, *J. Polym. Sci., Polym. Phys. Ed.*, **19**, 1865 (1981).
10. K. Kaji, I. Sakurada, K. Nakamae, T. Shintaku, and E. Shikata, *Bull. Inst. Chem. Res. Kyoto Univ.*, **52**, 308 (1974).
11. Z. W. Wilchinsky, *Advances in X-Ray Analysis*, Plenum, New York, 1963, Vol. 6, p. 231.
12. I. K. Park and H. D. Noether, *Colloid Polym. Sci.*, **253**, 824 (1975).
13. Y. Shimizu, K. Miyasaka, and K. Ishikawa, *Sen-i Gakkaishi*, **35**, T-507 (1979).
14. Y. Shimizu, H. Akabane, A. Tanioka, K. Miyasaka, and K. Ishikawa, *J. Polym. Sci., Polym. Phys. Ed.*, **17**, 1495 (1979).
15. H. R. Brown and E. J. Kramer, *J. Macromol. Sci. Phys.*, **B19**, 487 (1981).
16. E. Parades and E. W. Fischer, *Makromol. Chem.*, **180**, 2707 (1979).
17. A. V. Sidorovich and Yu. S. Nadezhin, *J. Macromol. Sci. Phys.*, **B16**, 35 (1979).
18. R. Hosemann and S. N. Bagchi, *Direct Analysis of Diffraction by Matter*, North-Holland, Amsterdam, 1962, Chap. 3.
19. H. Čačković, J. Loboda-Čačković, and R. Hosemann, *J. Macromol. Sci. Phys.*, **B16**, 145 (1979).
20. R. Hosemann and H. Čačković, *Colloid Polym. Sci.*, **259**, 15 (1981).
21. T. Tanigami, K. Yamaura, S. Matsuzawa, and K. Miyasaka, *Polym. J.*, **18**, 35 (1986).
22. H. H. Kausch, *Kunststoffe*, **66**, 538 (1976).

Received September 17, 1985
Accepted November 12, 1985